Indian Journal of Tribology Vol. 4(2) : 30-37, July-December, 2009
Copyright © Tribology Society of India 2009

Theoretical Predictions and Comparison of Oil Film Thickness, Pressure and Dynamic Characteristics of a Tilting Pad Thrust Bearing in Large Vertical Machines

D.V. SRIKANTH
Associate Professor in Mechanical Engineering
Bharat Institute of Engineering and Technology
Mangalpally, Hyderabad, A.P.
dvsrikanth1@hotmail.com

Dr. K.K. CHATURVEDI
Senior DGM, BHEL (R & D)
Vikas Nagar, Hyderabad, A.P.
chaturvedi@bhelrnd.co.in

Dr. A. CHENNA KESAVA REDDY
Professor in Mechanical Engineering
JNTU Engineering College, Ananthapur, A.P.
dracreddy@yahoo.com

In the present study, formulation of the oil film shape for a flat sector-shaped bearing surface is done. The thrust segment enables change of the oil film geometry and maintains its optimum shape even with varying load. Two dimensional Reynolds' equation is formulated for this bearing. Finite difference method is used to convert the Reynolds' equation terms into a set of simultaneous linear algebraic equations. A solution procedure for finding the pressure value in the oil film is described.

Numerical integration of the pressure values gives the load distribution. A detailed comparison of the present authors' and Ettles' numerical predictions with that of Yuans' experimental data showed good overall agreement. Subsequently, the study of dynamic characteristics of bearing like non-dimensional stiffness and damping is done by varying the value of the oil film thickness and introducing vertical velocity in the runner.

Keywords: oil film, pressure, dynamic characteristics, finite difference methods.

NOMENCLATURE

a : oil film shape parameter
h : oil film thickness, m
h_i : oil film thickness at leading edge, m
h_o : oil film thickness at the trailing edge, m
i : index of the node in radial direction
j : index of the node in circumferential direction
m : number of the nodes on the grid in radial direction
n : number of the nodes in circumferential direction coordinate along n -axis.
p : pressure in the oil film, Pa
r : radius of the runner, m
r_i : inner radius of the thrust pad, m
r_m : radial coordinate of the centre of pressure, m
r_o : outer radius of the thrust pad, m
t : transit time ,B/U, s
A1 . A2, A3 : coefficients for equation of a plane
B : circumferential length of the thrust segment, m
C_z : bearing damping coefficient, N-s/m
C_z* : non-dimensional damping coefficient
D_i : inner diameter of the thrust bearing, m
D_o : outer diameter of the thrust bearing, m
F_φ, F_z, F_y : viscosity integrals in the Reynolds' equation
G_p : gap between the pads, m
H : non-dimensional thickness of the oil film, h/ho
K_z : bearing stiffness coefficient, N/m
K_z* : non-dimensional stiffness coefficient
L : radial length of the thrust pad, m
N : angular speed of the runner, rpm
P : pressure matrix in Reynolds' equation
R : non - dimensional radius, r/r_o
R_{cp} : radial coordinate of the centre of pressure, m
U, V : velocity along and normal to surface, m/s
W : load on bearing, N
Z : no. of pads
γ : film thickness ratio
μ : viscosity of oil, Pa.s
θ : angle from the leading edge, radian
θ_{cp} : angular location of the centre of pressure, radian.
ρ : density of oil, kg/m3
ω : angular speed of the runner, radian /s
Δr : division on the grid along radial direction, m
Δv : volume of an element of the grid, m^3
$\Delta\theta$: angular division of the grid, radian.
ζ : coordinate along the z- axis
$\bar{\zeta}$: mean value of ζ

1. INTRODUCTION

A major component in the turbine assemblies of hydroelectric power stations is the thrust bearing. The thrust bearing carries the weight of the generator components and the hydraulic turbine plus the vertical hydraulic thrust load. The thrust load is transmitted from the rotor to the stator through lubricant oil films that develop between a rotating collar on the shaft and the stationary sector pads in the thrust bearing. Figure 1 illustrates the geometry of the thrust pad for large thrust bearings. The present work encompasses the first stage of research activity aimed at understanding the phenomena involved in the working of thrust bearing tilting pads. The rotor of a hydroelectric generator must move with low friction under the high load associated with its own weight and the hydraulic thrust. The bearing pads are supported by either a pivot or a distributed spring mattress. The support arrangements enable the pad to tilt

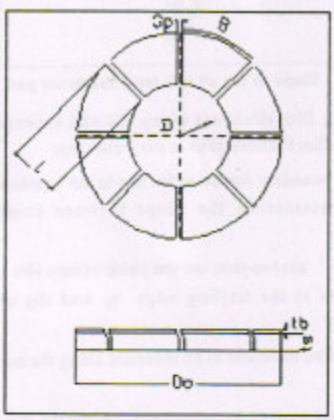

Fig. 1: Geometry of the thrust pad

and produce a lubricant film which maintains equilibrium between the generated and applied forces and moments. Large thrust bearings in hydroelectric generators have used spring-supported sector pads as an alternative to pivot-supported pads. The application of the more complicated spring supports is common in thrust bearings with outside diameters of more than 1 m. The present study examined sector pads supported by springs as shown in figure 2. One advantage of the distributed spring support, especially with the larger size of bearing is the ability to reduce the deflections of the pad.

An improved understanding of the hydrodynamics of the oil film and methods of calculation are essential to predict performance and design such bearings. Numerical models designing thrust bearings for the given operating conditions introduce an element of risk due to the shortage of experimental data available to check for accuracy of these predictions. Therefore there is a need, to obtain experimental data over a wide range of operating conditions and to check with the numerical model predictions. A possible approach for existing bearing designers is to obtain field data for comparison with numerical models. A full-scale apparatus to perform laboratory experiments for the simultaneous representation of thermal and mechanical influences on fluid film formation is very expensive to build and operate. The lack of an integrated theoretical and experimental

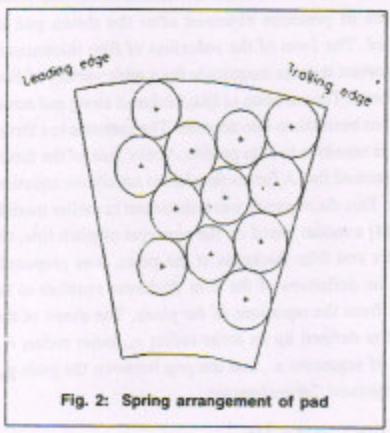

Fig. 2: Spring arrangement of pad

investigation has made the design of thrust bearings difficult. To develop design strategies of a large tilting pad thrust bearing there is a need for a realistic analytical model. It is essential that the predictions of this analytical model be compared with experiments that are realistic, comprehensive and allow sufficient parameter variations so as to check its fidelity. Otherwise it is almost certain that designs will be compromised by inaccuracies in the analytical model used to develop them. Therefore, the purpose of the present study is to determine the accuracy of the predictions of the authors' theoretical analysis for large tilting pad thrust bearings by comparing it with Ettles' numerical analysis [1] and Yuans' [2] experimental data.

Vohr (3) made the most recent attempt to perform such an analysis and include comparison with experiments for large thrust bearings. Although the agreement was good, Vohrs' analysis had certain inherent approximations. Detailed checks on Vohrs' analysis could not be performed without further experimental data, including pressure and oil film

thickness. The agreement between experiment and theory was to be maintained over a narrow range of operating conditions. Ettles' included the thermo elastic deflection of the pad for large thrust bearings using the bi-harmonic equation for plate bending.

2. GOVERNING EQUATIONS

2.i Shape of the oil film.

Operation of a tilting pad thrust bearing is based on the principle of a convergent wedge formed between two surfaces moving relatively. Due to shearing action of the runner, oil is dragged into it. Reduction of the cross-sectional area squeezes oil out of the trailing and side edges. The film thickness is considered to vary in circumferential and radial directions due to the roll and pitch motion of the pad, about the centre of pressure obtained after the thrust pad is assembled. The form of the reduction of film thickness is less important than its magnitude for a wide variety of film profile forms. The variation of film thickness along and across the pad has been taken into account. The pressure in a thrust bearing is sensitive to film profile. Active face of the thrust pad is assumed flat. A flat surface has to satisfy the equation of plane. This discrepancy was pointed out in earlier models and in [4] a model based on the concepts of pitch line, tilt parameter and film thickness at the pivot, was proposed. Hence, the definition of the film thickness requires to be derived, from the equations of the plane. The shape of the segment is defined by its outer radius r_o, inner radius r_i, number of segments z , and the gap between the pads g_p. Other important dimensions are

$$r_m = \left[\left(r_i^2 + r_o^2\right)/2\right]^{1/2} \qquad (1)$$

The angle subtended by the thrust segment at r_m is given by

$$\beta = 2\Pi/z - 2\sin^{-1}\left(g_p / 2r_m\right) \qquad (2)$$

Film shape parameter for the Mitchell shape of the film is defined as:

$$a = \left(h_i - h_o\right)/h_0 = \left[\left(h_i - h_o\right)/B \mid B/h_0\right]$$

The film shape for a flat pad is defined by the following equation, where the oil film is convergent in positive directions of x and y axes

$$h = A1 - A2x - A3y \qquad (3)$$

for $x = r\sin\left(\theta - \theta_{cp}\right)$ and $y = r\cos\left(\theta - \theta_{cp}\right) - r_{cp}$

The centre –of-pressure is assumed to be the origin. The coefficients A1, A2 and A3 are determined by specifying the following boundary conditions.

a) It is seen in figure 3 that film thickness at Q is the minimum film thickness h_o and using this boundary condition h_o in the equation (3).

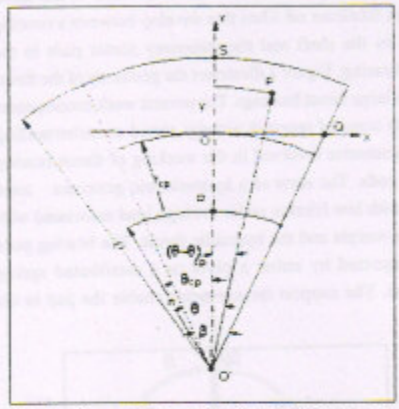

Fig. 3 : Shape of the oil film for a flat thrust pad

b) By using film thickness along RS and expressing γ' as the film thickness ratio in the y-direction

c) Another boundary condition for use in the equation (3) is by considering the slope between points O and Q.

d) Splitting γ' into two parts, one that yields uniform film thickness at the trailing edge γ_0 and the other variable γ.

e) Making film thickness to be invariant along the trailing edge.

Thus, the final form of the equation governing the shape of the oil film is given by

$$h = h_o\left[1 + \left(ar_{cp} / B\right)\tan\left(\beta - \theta_{cp}\right)\right]$$

$$-\left(ah_o / B\right)r\sin\left(\theta - \theta_{cp}\right)$$

$$+h_o\left[\left(a/B\right)\tan\left(\beta - \theta_{cp}\right) - \gamma/L\right]$$

$$\left[r\cos\left(\theta - \theta_{cp}\right) - r_{cp}\right] \qquad (4)$$

Equation for non-dimensional thickness of the oil film is:

$$H = h/h_o = 1 + \left(ar_{cp}/B\right)\tan\left(\beta-\theta_{cp}\right) - (ar/B)\sin\left(\theta-\theta_{cp}\right) + \left[(a/B)\tan\left(\beta-\theta_{cp}\right) - \gamma/L\right]\left[r\cos\left(\theta-\theta_{cp}\right) - r_{cp}\right] \quad (5)$$

2.2. Reynolds' Equation

The analysis of hydrodynamic thrust bearings have been based on Reynolds' equation for the pressure distribution. With the increasing capacity of computers, numerical models including the influences of viscosity variations along and across the lubricating film have been developed. Deformation of the bearing pads due to pressure and thermal gradients were also considered.

If only the lowest order terms are retained, these can be introduced in the continuity equation which is then integrated across the fluid film to give the Reynolds' equation. The temperature of the runner along its runner surface varies much less than the temperature in the thrust pad active face. The 'flash' temperature of the runner varies by less then 1 °C and the temperature along thrust pad rises by 15 to 20 °C as in [5]. Values of viscosity obtained from the temperature field in the oil film are substituted in the Reynolds' equation, to determine the pressure field. In load estimation the pressure 'fitting' at the edges has been made more appropriate to suit realistic conditions as in [6].

The generalized Reynolds' equation for rectangular thrust segment is:

$$\frac{\partial}{\partial x}\left[F_2\frac{\partial p}{\partial x}\right] + \frac{\partial}{\partial y}\left[F_2\frac{\partial p}{\partial y}\right] = \frac{\partial}{\partial y}\left[\frac{F_3}{F_0}U\right] \quad (6)$$

Where, $F_0 = \int_0^h \frac{d\zeta}{\mu}$

$$F_2 = \rho\int_0^h \frac{\zeta}{\mu}\left(\zeta - \bar{\zeta}\right)d\zeta$$

$$F_3 = \rho\int_0^h (\zeta/\mu)d\zeta$$

$$\bar{\zeta} = \int_0^h (\zeta/\mu)d\zeta \Big/ \int_0^h (d\zeta/\mu)$$

F_0, F_2 and F_3 are the viscosity integrals with units of m³.sec/kg, m.sec and sec respectively. Neglecting variation of viscosity across the thickness of the film, the Reynolds' equation for a sector-shaped thrust segment for incompressible lubricant, under steady state condition is derived as in

$$\frac{\partial}{\partial r}\left[\frac{rh^3}{\mu}\frac{\partial p}{\partial r}\right] + \frac{1}{r}\frac{\partial}{\partial\theta}\left[\frac{h^3}{\mu}\frac{\partial p}{\partial\theta}\right] = 6\omega r\frac{\partial h}{\partial\theta} + 12r\frac{\partial h}{\partial t} \quad (7)$$

Usual assumptions are made in the analysis done herein. The Reynolds' equation in non-dimensional form is:

$$2\frac{\partial}{\partial R}\left[\frac{RH^3}{\bar{\mu}}\right]\frac{\partial p}{\partial R} + \frac{2RH^3}{\bar{\mu}}\frac{\partial^2 P}{\partial R^2} + \frac{2}{\beta^2 R}\frac{\partial P}{\partial\bar{\theta}}\frac{\partial}{\partial\theta}\left[\frac{H^3}{\bar{\mu}}\right] + \frac{2}{\beta^2 R}\frac{H^3}{\bar{\mu}}\frac{\partial^2 P}{\partial\bar{\theta}^2} = 12R\frac{\partial H}{\partial\theta} + 24R\beta\frac{\partial H}{\partial t} \quad (8)$$

As compared to the above form of the equation, better numerical accuracy can be obtained, if all the first derivative terms in the equation are converted in to second derivative terms. Adopting this procedure the following equation is obtained.

$$\frac{\partial^2}{\partial R^2}\left[\frac{RH^3 p}{\bar{\mu}}\right] + \frac{RH^3}{\bar{\mu}}\frac{\partial^2 P}{\partial R^2} - P\frac{\partial^2}{\partial R^2}\left[\frac{RH^3}{\bar{\mu}}\right] + \frac{1}{R\beta^2}\frac{\partial^2}{\partial\bar{\theta}^2}\left[\frac{H^3 P}{\bar{\mu}}\right] + \frac{1}{R\beta^2}\frac{H^3}{\bar{\mu}}\frac{\partial^2 P}{\partial\bar{\theta}^2} - \frac{P}{R\beta^2}\frac{\partial^2}{\partial\bar{\theta}^2}\left[\frac{H^3}{\bar{\mu}}\right] = 12R\frac{\partial H}{\partial\theta} + 24R\beta V \quad (9)$$

3. COMPUTATIONAL PROCEDURE

Solution of Reynolds' equation using finite difference discretization of thrust pad is done by considering a total of 81 nodes in the form of a grid as shown in figure 4. The Reynolds' equation is a non-homogeneous partial differential equation of two variables for which closed form analytical solutions are not available. The use of finite difference methods for a numerical approximation of this type of partial differential equation is discussed in [7].

The finite difference equation is derived by approximating the derivatives in the differential equation via the truncated Taylor series expansion for three successive grid points. The central difference form where in the values of the

function at adjacent nodes on either side are required to evaluate the derivatives is used. Writing the Reynolds' equation in the above finite difference form as in equation (10) results in a set of linear algebraic equations which can be transformed into matrix form and solved simultaneously by available subroutines. This yields the non-dimensional pressure at each node.

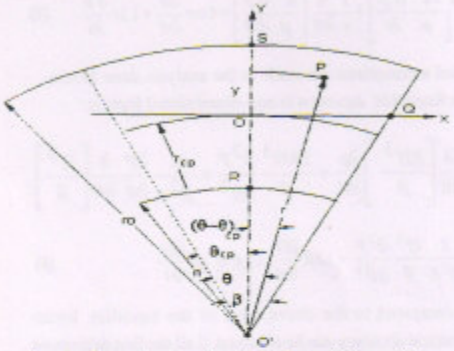

Fig. 4 : Discretization of pad for Reynolds' equation

$$P_{i+1,j}\left[\frac{R_{i,j}H_{i,j}^3}{\Delta R^2\bar{\mu}_{i,j}}+\frac{R_{i+1,j}H_{i+1,j}^3}{\bar{\mu}_{i+1,j}\Delta R^2}\right]$$

$$+P_{i-1,j}\left[\frac{R_{i,j}H_{i,j}^3}{\Delta R^2\bar{\mu}_{i,j}}+\frac{R_{i-1,j}H_{i-1,j}^3}{\bar{\mu}_{i-1,j}\Delta R^2}\right]$$

$$+P_{i,j+1}\left[\frac{H_{i,j}^3}{R_{i,j}\bar{\mu}_{i,j}\beta^2\Delta\bar{\theta}^2}+\frac{H_{i,j+1}^3}{R_{i,j}\bar{\mu}_{i,j+1}\beta^2\Delta\bar{\theta}^2}\right]$$

$$+P_{i,j-1}\left[\frac{H_{i,j}^3}{R_{i,j}\bar{\mu}_{i,j}\beta^2\Delta\bar{\theta}^2}+\frac{H_{i,j-1}^3}{R_{i,j}\bar{\mu}_{i,j-1}\beta^2\Delta\bar{\theta}^2}\right]$$

$$+P_{i,j}\left[-2\frac{R_{i,j}}{\Delta R^2}\frac{H_{i,j}^3}{\bar{\mu}_{i,j}}-\frac{R_{i+1,j}}{\bar{\mu}_{i+1,j}}\frac{H_{i+1,j}^3}{\Delta R^2}-\frac{R_{i-1,j}}{\bar{\mu}_{i-1,j}}\frac{H_{i-1,j}^3}{\Delta R^2}\right.$$

$$\left.-2\frac{H_{i,j}^3}{R_{i,j}\bar{\mu}_{i,j}\beta^2\Delta\bar{\theta}^2}-\frac{H_{i,j-1}^3}{R_{i,j}\bar{\mu}_{i,j+1}\beta^2\Delta\bar{\theta}^2}-\frac{H_{i,j-1}^3}{R_{i,j}\bar{\mu}_{i,j-1}\beta^2\Delta\bar{\theta}^2}\right]$$

$$=\frac{6R_{i,j}}{\Delta\theta}\left[H_{i,j+1}-H_{i,j-1}\right]+12R_{i,j}\bar{\beta}V \qquad (10)$$

The calculation procedure uses these calculated pressures along with numerical methods for integration to obtain the load capacity, radial and angular location of centre of pressure. To ensure numerical accuracy the pressure

4. DYNAMIC COEFFFICIENTS

a) The damping of the fluid film is its ability to absorb energy and is measured in N.sec/m.

The damping coefficient, C_z, is calculated using

$$C_z=\frac{\Delta W}{\Delta V} \qquad (11)$$

The subscript 'z' refers to the vertical direction of motion. Here W is the component of force causing displacement measured in N, and V is the vertical velocity measured in m/s. The formula for calculation of non-dimensional damping coefficient as in [8] is

$$C_z{}^*=C_z\frac{U}{L}\left[\frac{h_{min}{}^3}{BL^2U\mu_{eff}}\right] \qquad (12)$$

b) Similarly the stiffness of the fluid film is its ability to resist deformation by an applied force measured in N/m.

The stiffness coefficient, C_z, was calculated using

$$K_z=\frac{\Delta W}{\Delta h_o} \qquad (13)$$

where Δh_o is the change in minimum oil film thickness.

The formula for calculation of non-dimensional stiffness coefficient is

$$K_z{}^*=K_z\left[\frac{h_{min}{}^3}{BL^2U\mu_{eff}}\right] \qquad (14)$$

5. RESULTS AND DISCUSSIONS

TABLE 1: THRUST BEARING GEOMETRY

Outer Diameter (m)	1.168
Inner Diameter	0.711
Number of Pads	12
Thickness (mm)	30.2
Groove width (mm)	52.3
Number of Springs	12
Operating Conditions	
Load (MN)	2.124
Rotational speed (rads/s)	31.4
Oil pot temperature (°C)	70
Oil Properties	
ISO grade	32
γ(cSt) at 40 °C	33.55
γ(cSt) at 100° C	5.45

Table 1 lists the bearing geometry, operating conditions and oil properties. Oil properties used in the present software analysis did not correspond to those of the actual oils used in [9] but the influence of this inconsistency on the predictions was not significant. The present study and graphs aim to validate Vohrs' analysis and determines the accuracy of the present authors' analysis by comparing it with that of Ettles' and Yuans'[10].

Figure 5 shows the 3-dimensional pressure distribution obtained for the Mitchells' film shape and its model outlined in section 2.1. The pressure distribution near the trailing edge is identical. Near the leading edge, however, the pressure at the outer radius is slightly less than the value for the Mitchells' approximation. This is because of the lower oil film thickness for the Mitchell's model.

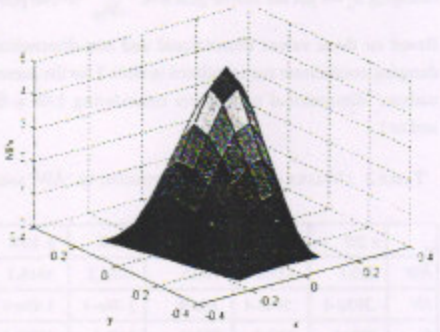

Fig. 5 : 3-D pressure distribution in the oil film of a flat pad

The agreement between film thickness is related to the agreements for pressures for the present authors', Ettles' and Yuans' predictions. Figures 6(a,b,c) show the agreement between theory and experiment achieved for the film thickness values measured for the three respective displacement probes. In Yuans' analysis discrete experimental values directly plotted from by the data acquisition system resulted in the scatter. The present authors' theoretical film thickness values compared well and were lower than Yuans' experimental values. Also variation of temperature in the oil film was not considered in the author's analysis.

Figure 6(a) showed that there was good agreement between the present authors' and Yuans' experimental film thicknesses and surface shape. This was because of a better output voltage corresponding to zero film thickness. Comparison between present authors' and Ettles' predictions showed good agreement. However the present authors' values were lower because thermo elastic deflection of the pad was not considered

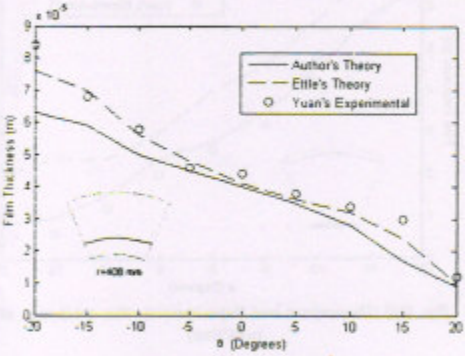

Fig. 6 (a): Theoretical and Experimental film thickness at r=408mm

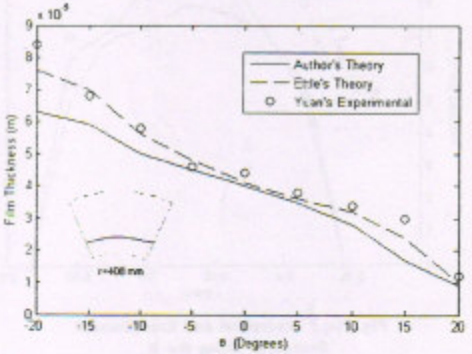

Fig. 6 (b) :Theoretical and Experimental film thickness at r=516mm

Figure 6(c) showed that Yuans' measured film thickness values gave a surface shape similar to the present authors' solution. In Figure's 7(a,b) the comparison between present authors' solution and Yuans' experimental pressure values showed that the measured values were slightly higher than those predicted by theory.

The reason is attributed to insignificant crowning, lower speed and viscosity. It was also likely that the present software package was underestimating pressure. The difference between the present authors' solution and Ettles' prediction was accounted for the inaccuracies in predicting the thermo elastic deformation of the rotor surface and thrust segment.

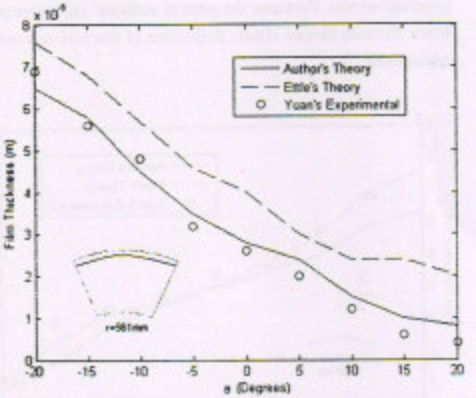

Fig. 6(c) :Theoretical and Experimental film thickness at r=581mm

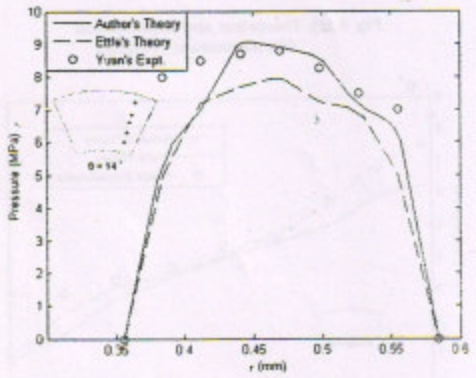

Fig. 7(a) : Theoretical and Experimental Pressures along the R_{ep}

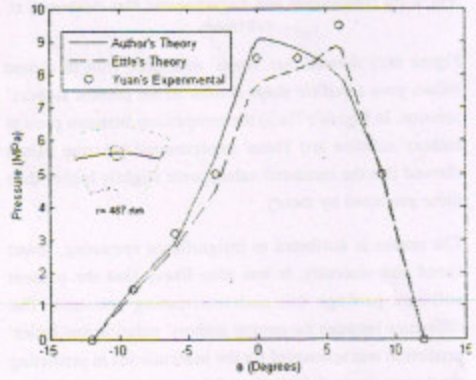

Fig. 7(b): Theoretical and Experimental Pressures from R_i to R_o

The input data used for calculation of damping and stiffness coefficients in the tilting – pad thrust bearing was $D_o = 1.275m, D_i = 0.75m, z = 6, G_p = 0.084, \dot{u} = 14.28$ radian/ sec, $h_o = 52.5e\text{-}6m$.

Initially we gradient film thickness coefficients by substituting the values of a and h_o in the equation for the oil film shape. By substituting these gradient film thicknesses in modified Reynolds' equation we get pressure at each node. Numerical integration to these pressure points gives the load. V and h_o values are varied from +10% to -10% and the change in values of W so obtained is denoted as ΔW. The reason for changing V values in decrements from 10 to 2% is to get the convergence of $\frac{\Delta W}{\Delta V}$ to one point and at ± 2% to get the correct asymptotic value. In a similar way changing h_o we get the convergence of $\frac{\Delta W}{\Delta h_o}$ to one point.

Based on these values dimensional and non-dimensional damping coefficients are calculated in table 2 for the present authors' dimensional parameters considering L/B = 0.7 and a=1.

TABLE 2 : VALUES OF 'C_z*' CORRESPONDING TO 'ÄW' AND 'ÄV'

	± 2%	± 4%	± 6%	± 8%	± 10%
ÄW	263.8	425.6	796.6	1068.2	1616.7
ÄV	.293e-4	.594e-4	.89e-4	1.49e-4	1.49e-4
C_z	888e4	716e4	894e4	717e4	1088e4
C_z*	1.4*10-8	3*10-8	3.7*10-8	3*10-8	4.5*10-8

For the same 'L/B' and 'a' values table 3 shows the corresponding stiffness values calculated for different values of ΔW *and* Δh_o.

TABLE 3 : VALUES OF 'K_z*' CORRESPONDING TO 'ÄW' AND 'ÄH_o'

	± 2%	±4%	±6%	±8%	±10%
ÄW	263.8	425.6	796.6	1068.2	1616.7
ÄV	.0052	.0104	.0156	.0208	.0260
C_z	50678	40880	51011	51302	62116
C_z*	5.0*10-9	4.0*10-9	5.0*10-9	5.0*10-9	6.1*10-9

Figures 8 and 9 show non-dimensional damping and stiffness coefficient contour plots respectively for 'a' varied from 1.0 to 2.2 and L/B from 0.7 to 1.3.

The present authors' non-dimensional damping coefficient value at L/B = 0.7 and a=1 is 4.3114e-18 and decreases gradually as 'a' and L/B are increased and finally at a = 2.2 and L/B = 1.3 the value becomes 1.5006 e-18. The value of the non-dimensional stiffness coefficient at L/B = 0.7 and 'a' = 1.0 is 1.6006e-20 and increases gradually and at 'a'= 2.2 and L/B = 1.3 is equal to 4.5713e-21

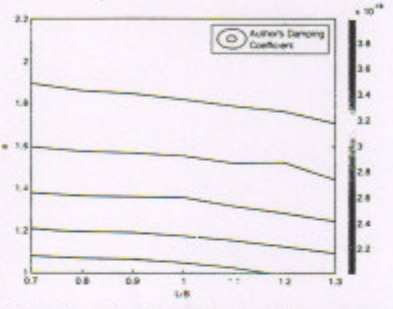

Fig. 8: Non-Dimensional Damping C_z * with respect to Film shape parameter *a* and *L/B* ratio

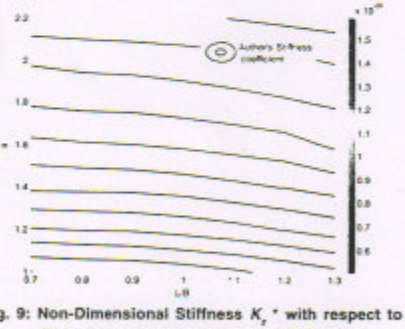

Fig. 9: Non-Dimensional Stiffness K_z * with respect to Film shape parameter *a* and *L/B* Ratio

6. CONCLUSIONS:

Formulation of the oil film shape and variation of film thickness along and across the flat sector pad is done. Modified two dimensional Reynolds' equation and a finite difference solution procedure for finding pressure values is written and verified. Numerical integration to these pressure points gives the load. Good agreement occurred between the theoretical and experimental film thicknesses. For the cases considered experimental pressures were usually higher than those predicted by theory. The differences in pressures might have been caused by rotor crowning giving thicker films than predicted by theory at the outer edge of the bearing. and inaccuracies in the thermo elastic deflection model of Ettles' predictions. No thermo elastic deflection and variation in temperature of the oil film was considered in the present authors' analysis. Subsequently the non-dimensional damping and stiffness coefficients for the variation of film thickness and introduction of vertical velocity were determined.

Agreement between theoretical and experimental results although not perfect did provide solid support for the utility of the two software packages used in predicting large spring-supported thrust bearing behaviour. These data are a useful input for the rotor dynamic studies.

7. REFERENCES:

1. Ettles C., "Some Factors Affecting the Design of Spring Supported Thrust Bearings in Hydroelectric Generators", Journal of Tribology, Trans. of the ASME. Vol.113. No.6, (1991), pp. 626-632, July.

2. Yuan J.H., Ferguson J.H. and Medley J.B., "Spring Supported Thrust Bearings used in Hydroelectric Generators: Labratory testing Facility", STLE Tribology Transactions, January, (1999), pp.126-135.

3. Vohr J.H , "Prediction of the Operating Temperature of Thrust Bearings", ASME , Journal of Lubrication Technology, 103, (1981), pp.97-106.

4. Etsion I., : Design Charts for Arbitrarily – Pivoted , Liquid Lubricated, Flat Sector-Pad Thrust Bearing, Journal of Lubrication Technology, Transactions of the ASME , Vol. 100, (1978), pp.279-286, April.

5. Ettles C.M.M. and Anderson , H.G., "Three – Dimensional Thermo - Elastic solutions of thrust bearings using code Marmac 1", Journal of Tribology , Transactions of the ASME , vol. 112, (1991), pp.405- 412.

6. Chaturvedi K.K., Athre K., Nath Y, and Biswas S, "Refinement in Estimation of Load Capacity and Temperature Distribution of Pad Bearing," Proceedings of Eurotrib-89, (1989), Helisinki, Finland, June.

7. Capitao J.W, "Influence of Turbulence on Performance Characteristics of the Tilting Pad Thrust Bearing", Transactions of the ASME, Journal of Lubrication Technology, January, (1974), pp.110-117.

8. Eskild Storteig, Maurice F. White, "Dynamic Characteristics of hydrodynamically lubricated fixed-pad thrust bearings", Wear vol. 232, (1999), pp.250-255.

9. Yuan J.H., Ferguson J.H. and Medley J.B., "Spring Supported Thrust Bearings for Hydroelectric Generators: Influence of oil viscosity on power loss", Proceedings Energy Conservation in Trib. Series , 24. Elsevier. (1998). pp.187-194.

10. Yuan J.H., Ferguson J.H. and Medley J.B., "Spring Supported Thrust Bearings Hydroelectric Generators: Comparison of